EXPERIMENTAL AND COMPUTATIONAL INVESTIGATION OF PIEZOCERAMIC ACTUATOR HYSTERESIS PHENOMENON IN HELICOPTER VIBRATION CONTROL USING DUAL TRAILING-EDGE FLAPS

S.R.Viswamurthy[1] and R. Ganguli[2]

[1] Department of Aerospace Engineering
Indian Institute of Science, Bangalore-560012, India
e-mail: murthy@aero.iisc.ernet.in

[2] Department of Aerospace Engineering
Indian Institute of Science, Bangalore-560012, India
e-mail: ganguli@aero.iisc.ernet.in

Key words: Vibration control, piezoceramic actuator, hysteresis, dynamic hysteresis model

Abstract: This study investigates the effect of piezoceramic actuator hysteresis on helicopter vibration control using dual trailing-edge flaps. Piezoceramic stack actuators are promising candidates for trailing-edge flap actuation in full-scale helicopters. However, they are inherently nonlinear in response to an applied electric field and exhibit hysteretic behavior between the applied electric field and displacement. In this study, bench top tests were conducted on a commercially available piezoceramic stack actuator and its hysteretic behavior is studied. A Preisach type dynamic hysteresis model is used to describe the hysteresis in the stack actuator. The unknown coefficients in the model are obtained through identification from experimental data. An aeroelastic model of the helicopter with multiple trailing-edge flaps is then used to predict the hub vibration levels under different flight conditions. The optimal actuator control input for hub vibration suppression in the presence of hysteresis is considerably different from the case of an ideal-linear actuator. Numerical results show the importance of modeling actuator hysteresis in helicopter vibration control using trailing-edge flaps. Ignoring or inaccurate modeling of hysteresis in the piezoceramic actuator can lead to inaccurate phasing of the trailing-edge flap motion which directly affects the performance of the vibration control system.

1 INTRODUCTION

Vibration is a key issue in rotorcraft and studies indicate that active trailing-edge flaps have great potential in the field of rotorcraft vibration suppression [1,2]. This concept is attractive since it does not interfere with the operation of helicopter primary control system. These flaps are typically moved at higher harmonics of the rotor rotational speed to reduce vibration at the rotor hub. Recent studies show that multiple flaps have the advantage of flexibility over rotor blades with single trailing-edge flap [3]. Piezoceramic stack actuators are ideally suited for actuation of such trailing-edge flaps. They are light, compact, have high energy-density and high bandwidth. Lee and Chopra successfully demonstrated the performance of a piezostack based actuation device in conjunction with a double-lever (L-L) amplification mechanism through tests in an open-jet wind tunnel [4]. In another study, Hall and Prechtl developed a discrete trailing edge servo-flap actuator called an X-frame actuator and successfully conducted tests on a 1/6 Mach scaled model rotor system to demonstrate the actuator control authority [5].

However, a major limitation of piezoceramic stack actuators is their lack of accuracy due to hysteresis and drift. Piezoceramic materials are fundamentally nonlinear in their response to an applied electric field, exhibiting a hysteresis between the applied electric field and displacement. Hysteresis in piezoceramic materials is a form of nonlinearity with memory. Thus, the piezoceramic expansion depends not only on the current voltage excitation but also on the history of excitation. Not modeling hysteresis in the piezoceramic actuator can lead to inaccuracy in open-loop control and can lead to amplitude dependent phase shifts. Kurdila et al developed a nonlinear control methodology that accounts for the hysteresis in PZT actuated elevons [6]. However, they used a simple linear helicopter aeroelastic model and the objective was not vibration control. Viswamurthy and Ganguli studied the effect of piezoceramic hysteresis on helicopter vibration control using a single trailing-edge flap [7]. They used experimental data from Hall and Prechtl [5] to create a static model based on the classical Preisach model for the actuator hysteresis [8]. They concluded that the controller performance deteriorated in the presence of actuator hysteresis. Furthermore, it was shown that the control input for achieving the optimal flap motion is different in the case of a hysteretic actuator as compared to an ideal-linear actuator.

The classical Preisach model used in [7], though popular, has several limitations. The classical Preisach model (CPM) is static and rate independent in nature and is limited in describing dynamic hysteresis phenomena. In this study, a dynamic hysteresis model based on CPM is used to describe the hysteresis in a commercially available piezoceramic stack actuator. This model removes the rate-independency limitation of CPM. Bench-top experiments are conducted on a commercially available piezoceramic stack actuator (APA500L from CEDRAT Technologies) and this data is used to determine the unknown parameters in the dynamic hysteresis model. The hysteresis model is then cascaded with the nonlinear helicopter aeroelastic model. An optimal control law is then used to obtain the control input for achieving maximum reduction in hub vibration levels. The rest of the paper is organized in the following manner: Section 2 gives a brief description of the aeroelastic model of the helicopter rotor in forward flight. Section 3 contains some experimental results from the actuator bench-top test and establishes the need for a dynamic hysteresis model. Section 4 gives a brief introduction to the CPM and its extension to a dynamic hysteresis model. Section 5 describes the actuator control algorithm used in this study. Finally, numerical results and discussion are given in Section 6.

2 HELICOPTER AEROELASTIC ANALYSIS

2.1 Structural model

The helicopter is represented by a nonlinear aeroelastic model of several elastic rotor blades dynamically coupled to a rigid fuselage. Each blade undergoes flap bending, lag bending, elastic twist and axial displacement. Small strains and finite rotations (moderate deflections) are assumed and the Euler-Bernoulli hypothesis is used. The trailing-edge flaps are assumed to be an integral part of the blade. The trailing-edge flap hinge is assumed to coincide with its leading edge. The flap hinges are assumed to be rigid in all directions except about the hinge axis, thereby allowing only pure rotation of the flap in the plane of the blade cross-section. It is also assumed that the flaps do not contribute to the stiffness of the rotor blade and influences the behavior of the blade only through its contribution to the blade spanwise aerodynamic and inertial loading.

2.2 Aerodynamic model

The aerodynamic forces and moments acting on the blade section are calculated for unsteady profile and flap motion in the forward flight condition. The attached flow formulation is based on the indicial response method in which response is calculated from a finite difference approximation to the Duhamel's integral. Compressibility effects are implicitly included in the indicial response functions [9]. A time domain unsteady aerodynamic model developed by Hariharan and Leishman for a flapped airfoil in compressible, subsonic flow is utilized [10]. The formulation is based on linearization of the governing partial differential equations similar to that applied in classical thin airfoil theory. The present analysis considers the incremental effects on flap and profile aerodynamics caused by trailing edge flap motions. A free-wake model is used to determine the induced inflow distribution over the rotor disk [11].

2.3 Formulation and solution procedure

The aeroelastic formulation is based on a generalized Hamilton's principle applicable to non-conservative systems:

$$\int_{\psi_1}^{\psi_2} (\delta U - \delta T - \delta W) d\psi = 0 \qquad (1)$$

δU , δT and δW are the virtual strain energy, kinetic energy and work, respectively. Finite element methodology is used to discretize the governing equations of motion. The beam is discretized into 10 finite elements and each of these 10 beam finite elements has 15 degrees of freedom. The spatial functionality is removed by using finite element discretization and partial differential equations are converted to ordinary differential equations. In order to reduce the computational cost, the finite element equations in terms of the nodal displacements are transformed into modal space. Four flap, four lag and two torsion modes are used in this study. The blade response is solved in modal space using finite element in time. Eight time elements are used and fifth order polynomials are used as shape functions. A coupled trim/aeroelastic solution procedure is carried out to simultaneously solve for blade nonlinear steady response, pilot input trim controls and vehicle orientation. Steady and vibratory components of the rotating frame blade loads are calculated using force summation method. In this approach, blade inertia and aerodynamic forces are integrated directly over the length of the blade. Fixed frame hub loads are calculated by summing the contributions of individual blades at the root. The hub forces and moments are nondimensionalized with respect to $m_0 \Omega^2 R^2$ and $m_0 \Omega^2 R^3$, respectively. Additional details of the aeroelastic analysis are given in reference [12].

3 ACTUATOR BENCH-TOP TESTS

Bench-top experiments are conducted on a commercially available piezoceramic stack actuator. Figure 1 shows the APA500L actuator from CEDRAT Technologies under blocked-free condition. Figure 2 shows a schematic diagram of the experimental setup. The APA500L is a large-stroke, amplified piezo actuator which is suited for actuation of a full-scale trailing-edge flap. DSPACE controldesk is used to send command to the high-voltage amplifier required to power the APA500L actuator. An LVDT sensor is used to measure the displacement of the actuator and the data is collected using DSPACE for post-processing. The actuator displacement is converted to equivalent flap deflection by multiplying it with a known gain factor. This factor can be thought of as the gain of an ideal linear amplification mechanism with zero friction or nonlinearities.

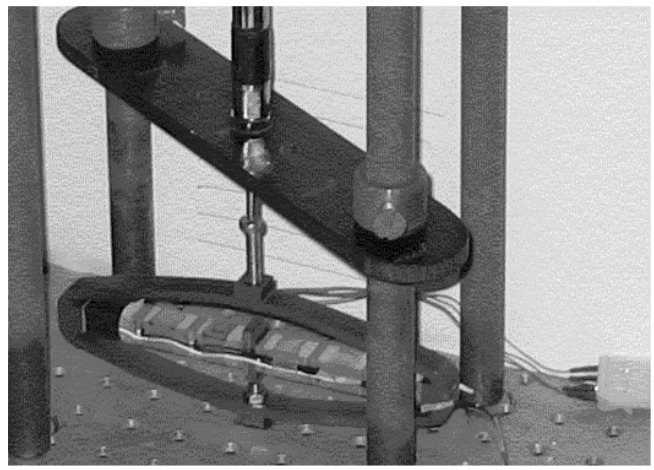

Figure 1: APA500L stack actuator under blocked-free condition

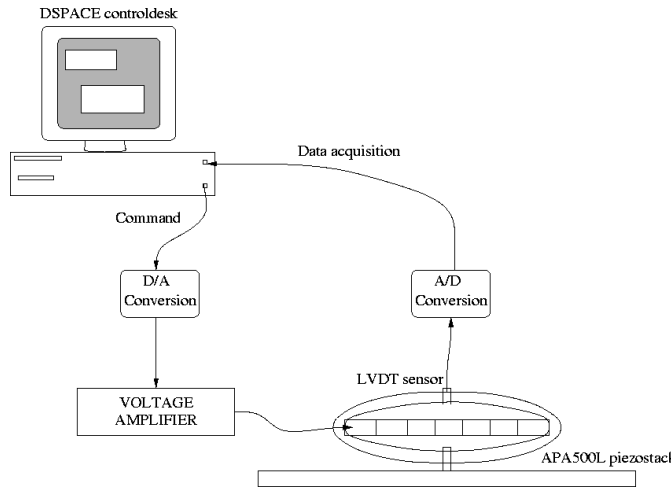

Figure 2: Experimental setup

Figure 3 shows the quasi-static response (actuation frequency ~ 0.2 Hz) of the actuator on the bench top. The amplification mechanism gain mentioned previously is set to a value such that

the peak-to-peak equivalent flap deflection under quasi-static conditions is ±10 degrees. This value of the gain is kept constant for the rest of the study. Clearly, the actuator is fairly nonlinear even under quasi-static conditions.

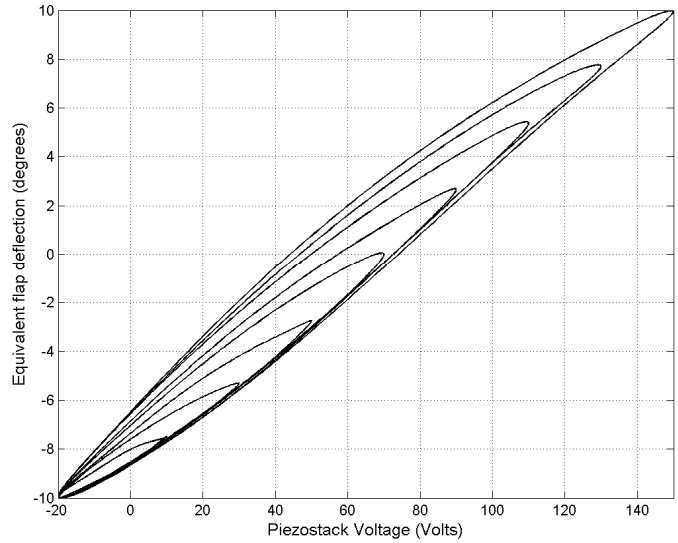

Figure 3: Quasi-static response of the stack actuator normalized to yield equivalent flap deflection

However, the trailing-edge flaps in the helicopter rotor are typically moved at higher harmonics (2, 3, 4 and 5/rev) of the rotor rotation speed which falls in the range of 10-30 Hz. Figure 4 shows the response of the actuator at several operational frequencies (1-20 Hz). It is clear that the ±10 degrees flap actuation at 0.2 Hz leads to an actuation of ±4 degrees at 15 Hz which is typical of current day stack actuators. Under the higher frequency conditions such as 10-20 Hz, the actuator response is considerably different from the response at quasi-static condition. It is evident that both the amplitude and phase of the response are dependent on the input amplitude and frequency. In other words, this actuator exhibits rate-dependent hysteresis phenomena which cannot be modeled accurately by the classical Preisach model. Hence, there is a need to develop a dynamic hysteresis model to describe the response characteristics of this actuator. This is addressed in the next section.

4 ACTUATOR HYSTERESIS MODEL

4.1 The classical Preisach model

The Preisach model was originally developed for describing hysteresis in ferromagnetic materials [8]. Krasnoselskii separated Preisach's model from its physical meaning and represented it in a pure mathematical form [13]. As a result, this model can now be used for the mathematical description of hysteresis of any physical nature. The Preisach model has several appealing features including its ability to model complex hysteresis types, a well defined identification algorithm, and a convenient numerical simulation form [14,15]. Several researchers have successfully applied the classical Preisach model to represent hysteresis in ferroelectric material systems. Sreeram and Naganathan were the first to apply the classical Preisach model to piezoceramic material system [16]. Hughes and Wen discussed and verified the applicability of Preisach model to piezoceramic and shape memory alloy systems [17]. Ge and Jouaneh

used a modified Preisach model to represent hysteresis in a stacked piezoceramic actuator and validated the model through experiments [18].

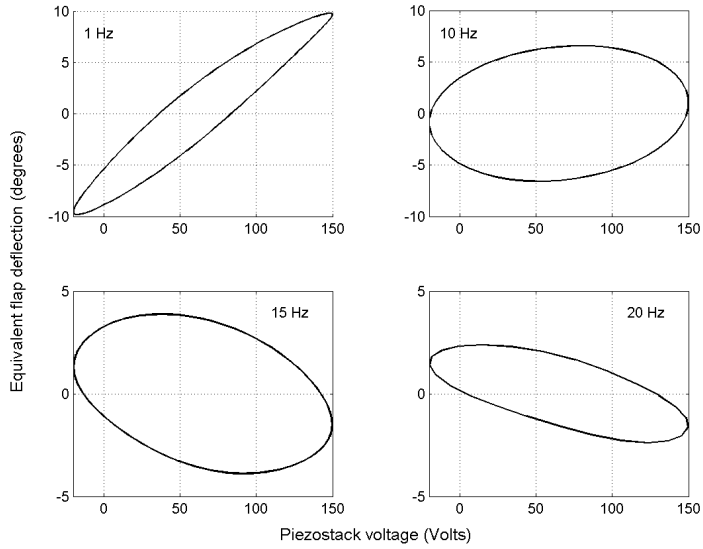

Figure 4: Actuator response at higher operational frequencies

The classical Preisach model can be seen as the superposition of a continuous set of two-position relays and can be written in the following mathematical form:

$$\delta(\psi) = \Gamma[u](\psi) = \iint_{\alpha \geq \beta} \mu(\alpha, \beta) \gamma_{\alpha\beta}[u](\psi) d\alpha d\beta \qquad (2)$$

where ψ is the non-dimensional time, $\delta(\psi)$ is the actuator response, $u(\psi)$ is the input-voltage signal, $\Gamma[u](\psi)$ is the Preisach operator, $\gamma_{\alpha\beta}$ are elementary hysteresis operators (elementary relay elements) with switching values α and β and whose values are determined by the input-voltage signal $u(\psi)$ (Figure 5). The function $\mu(\alpha, \beta)$ is a weighting function estimated from experimental data and is called the Preisach distribution function. If the Preisach distribution function is known, then equation (2) can be solved directly by integration to obtain the system output. If the function $\mu(\alpha, \beta)$ is not known explicitly, then experimental data is needed to estimate it [14, 15]. It is well-known that Γ fulfills the wiping-out and congruency properties [14, 15]. The integration in equation (2) is performed within the following limits: $u_{\min} \leq \beta \leq \alpha$ and $u_{\min} \leq \alpha \leq u_{\max}$ where $u_{\min}$ and $u_{\max}$ are the minimum and maximum values of the input-voltage signal. The reader is referred to [14, 15] for a detailed description of the classical Preisach model and its numerical implementation.

4.2 Dynamic hysteresis model and parameter identification

The classical Preisach model, though widely used, has several limitations. It is well-known that the Preisach model can be used to model only static hysteresis phenomena. The term 'static' means that the system output predicted depends only on the past extremum values of input, while the speed of the input variation between extremum points has no influence on the output [14]. This limits the applicability of this model to systems that exhibit rate-dependent hysteresis. To solve this issue, Mayergoyz proposed a new Preisach type hysteresis model that relaxes the 'static property' of the classical Preisach model [19].

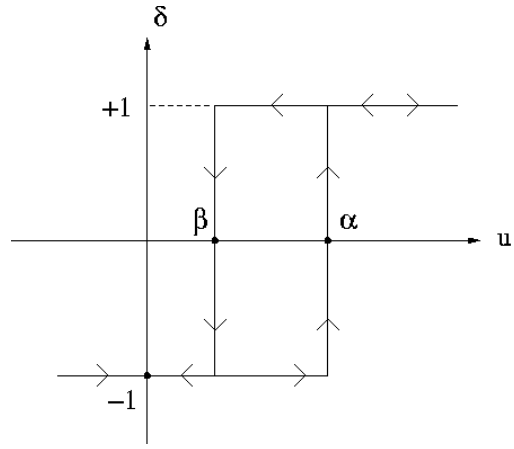

Figure 5: An elementary hysteresis operator

In the dynamic hysteresis model proposed by Mayergoyz, the static property is relaxed by introducing the dependence of Preisach distribution function (μ) in equation (2) on the speed of the output variations, $\left(\frac{d\delta}{d\psi}\right)$. The dynamic hysteresis model can be written as:

$$\delta(\psi) = \iint_{\alpha \geq \beta} \mu\left(\alpha, \beta, \frac{d\delta}{d\psi}\right) \gamma_{\alpha\beta}[u](\psi) d\alpha d\beta \qquad (3)$$

However, this model cannot be easily implemented since the distribution function μ depends on the unknown quantity $\left(\frac{d\delta}{d\psi}\right)$. This difficulty is overcome by using the Taylor series expansion for μ with respect to $\left(\frac{d\delta}{d\psi}\right)$:

$$\mu\left(\alpha, \beta, \frac{d\delta}{d\psi}\right) = \mu_0(\alpha, \beta) + \frac{d\delta}{d\psi}\mu_1(\alpha, \beta) + \frac{d^2\delta}{d\psi^2}\mu_2(\alpha, \beta) + \ldots \qquad (4)$$

The first three terms on the right-hand side of equation (4) are retained and substitution into equation (3) gives the following dynamic hysteresis model:

$$\begin{aligned} \delta(\psi) = & \iint_{\alpha \geq \beta} \mu_0(\alpha, \beta) \gamma_{\alpha\beta}[u](\psi) d\alpha d\beta + \frac{d\delta}{d\psi} \iint_{\alpha \geq \beta} \mu_1(\alpha, \beta) \gamma_{\alpha\beta}[u](\psi) d\alpha d\beta \\ & + \frac{d^2\delta}{d\psi^2} \iint_{\alpha \geq \beta} \mu_2(\alpha, \beta) \gamma_{\alpha\beta}[u](\psi) d\alpha d\beta \end{aligned} \qquad (5)$$

It is clear that in the case of very slow output variations, the above model reduces to the corresponding static model. This means that the function μ_0 is in fact the distribution function of the static Preisach model and can estimated using known methods [15]. In the current study, the function μ_0 is estimated based on the quasi-static response of the APA500L actuator (Figure 3). Further experiments were conducted at frequencies of 1 Hz and 10 Hz and the actuator output was measured. This experimental data is then used to estimate the unknown functions, μ_1 and μ_2, using a least-squares method.

4.3 Model validation

To verify and validate the dynamic hysteresis model identified in the previous section, we compare the actuator output from experiments conducted at higher frequencies with the output of the model (Figures 6 and 7). The dynamic hysteresis characteristics are captured very well at 10 Hz and 15 Hz which represent the 2/rev and 3/rev frequencies of a typical helicopter with Ω = 5 Hz. Agreement at 20 Hz is also quite good. We can see that they agree reasonably well and therefore the identified dynamic hysteresis model provides a good approximation to the actuator.

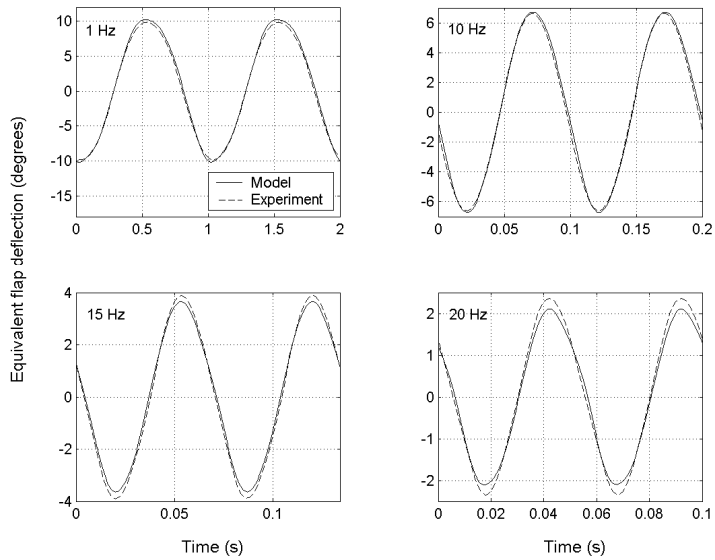

Figure 6: Measured and predicted actuator output at 1, 10, 15 and 20 Hz

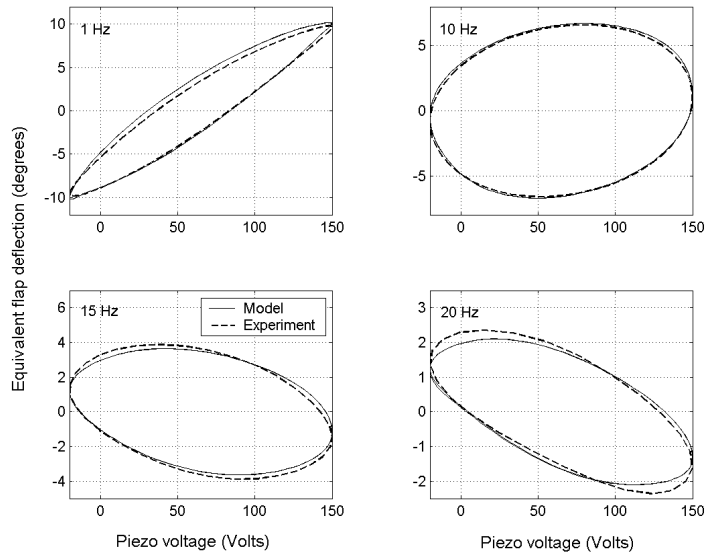

Figure 7: Measured and predicted output versus actuator input

5 CONTROL ALGORITHM

In the current study, a four bladed, soft inplane, uniform hingeless rotor similar to the BO105 rotor is considered. Each rotor blade has two trailing-edge flaps to introduce control input directly in the rotating reference frame (Figure 8). This configuration was chosen based on optimization studies with two objectives: (a) Hub vibration reduction capacity and (b) Trailing-edge flap actuation power. In steady forward flight, the helicopter rotor system can be assumed to be periodic in time. This periodic nature of the system allows us to transform the control problem from the time domain to the frequency domain [20]. The control algorithm is based on the minimization of an objective function that is a quadratic function of hub vibratory loads and control input magnitudes. In this study, the control input is the applied actuator voltage and not the flap deflection angle itself.

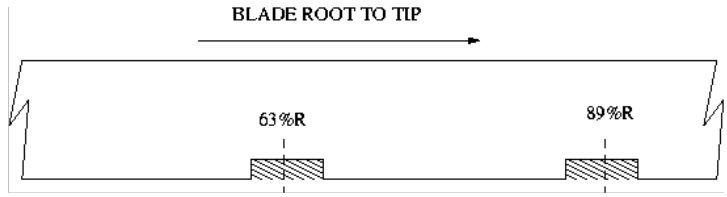

Figure 8: Schematic view of the rotor blade with dual trailing-edge flaps

For a four bladed rotor, the control input to the actuator is typically 2, 3, 4 or 5/rev or a combination of all the above harmonics to reduce the vibratory hub loads. In the current study, a DC bias is also given to the stack actuator. This DC bias is adjusted so as to obtain a flap motion with zero steady component. The total voltage applied to the piezostack is then given by:

$$u(\psi) = u_{st} + \sum_{N=2}^{5} \left[u_{Nc} \cos(N\psi) + u_{Ns} \sin(N\psi) \right] \qquad (6)$$

The objective function for optimal control is given by:

$$\begin{aligned} &J(\mathbf{Z}_i, \mathbf{u}_i) = \mathbf{Z}_i^T \mathbf{W}_Z \mathbf{Z}_i + \mathbf{u}_i^T \mathbf{W}_u \mathbf{u}_i \\ &\text{where, } \mathbf{Z}_i = [F_x F_y F_z M_x M_y M_z]_{4p}^T, \text{ and } \mathbf{u}_i = [u_{2c} u_{2s} u_{3c} u_{3s} u_{4c} u_{4s} u_{5c} u_{5s}]^T \end{aligned} \qquad (7)$$

The subscript i in equation (7) refers to the i^{th} control step, reflecting the discrete-time nature of the control. The time interval between each control step must be sufficient to allow the system to return to the steady state so that the vibration level can be measured accurately. A linear, quasi-static, frequency domain representation of helicopter response to control input is generally used in the minimization of the objective function [21]. Since u_{st} is not an independent parameter, it is not included in the vector of control input harmonics, $\mathbf{u}_i$.

In this study, the "feedback form of the global controller" is used to determine the optimal control input [22]. The transfer matrix ($\mathbf{T}$) is assumed to be constant over the entire range of control inputs. This controller is a closed-loop form where the control input during each control step is determined by feedback of the measured vibration levels of the previous control step. Linearizing the system about the current control inputs using Taylor series expansion gives:

$$\mathbf{Z}_i = \mathbf{Z}_{i-1} + \mathbf{T}_0 (\mathbf{u}_i - \mathbf{u}_{i-1}) \qquad (8)$$

$\mathbf{T}_0$ is the transfer matrix which is numerically computed by perturbing the control harmonics about the zero values and using a finite difference method. Equation (8) is substituted in equation (7) and the following optimality criteria in applied:

$$\frac{\partial J}{\partial \mathbf{u}_i} = \mathbf{0} \qquad (9)$$

The optimal controller then becomes,

$$\begin{aligned} \mathbf{u}_i^* &= \mathbf{C}_0 \mathbf{Z}_{i-1} - \mathbf{C}_0 \mathbf{T}_0 \mathbf{u}_{i-1} \\ \text{where, } \mathbf{C}_0 &= -\mathbf{D}_0 \mathbf{T}_0^T \mathbf{W}_Z \text{ and } \mathbf{D}_0 = \left(\mathbf{T}_0^T \mathbf{W}_Z \mathbf{T}_0 + \mathbf{W}_u\right)^{-1} \end{aligned} \qquad (10)$$

6 NUMERICAL RESULTS AND DISCUSSION

The helicopter rotor blade and trailing-edge flap properties considered in this study are shown in Table 1. Numerical results are obtained at a forward speed corresponding to an advance ratio of 0.30.

Table 1: Rotor blade and trailing-edge flap properties

Blade properties	
N_b	4
c/R	0.055
Solidity, σ	0.07
Lock number, γ	5.20
C_T/σ	0.07
$EI_y/m_0\Omega^2R^2$	0.0108
$EI_z/m_0\Omega^2R^2$	0.0268
$GJ/m_0\Omega^2R^2$	0.00615
$m_0, kg/m$	6.46
Ω, rpm	383
R, m	4.94
Trailing-edge flap properties	
c_f/c	0.20
m_f/m_0	0.10
X_g^f/c_f	0.20

Initial studies are conducted by applying the higher harmonics of the control input individually. In this case, the total number of unknown control input harmonics is four (two per flap), which can determined from equation (10). The optimal 2/rev control input and the resulting flap motion for the inboard and outboard flaps are shown in Figure 9. It can be seen that the outboard flap motion leads the inboard flap by about 65 degrees. The helicopter aeroelastic analysis predicts about 29 percent reduction in hub vibration levels for this case. Also, the actuator response (flap motion) lags the control input (applied voltage) by about 47 degrees for both flaps. Clearly, this phase difference is due to the hysteresis in the actuator which is

dependent on both the amplitude and frequency of the input voltage. Hence, ignoring the actuator hysteresis or using a linear model for the actuator will almost certainly lead to erroneous prediction in the optimal control input. This in turn will lead to non-optimal flap motion which will directly affect the performance of the trailing-edge flap system.

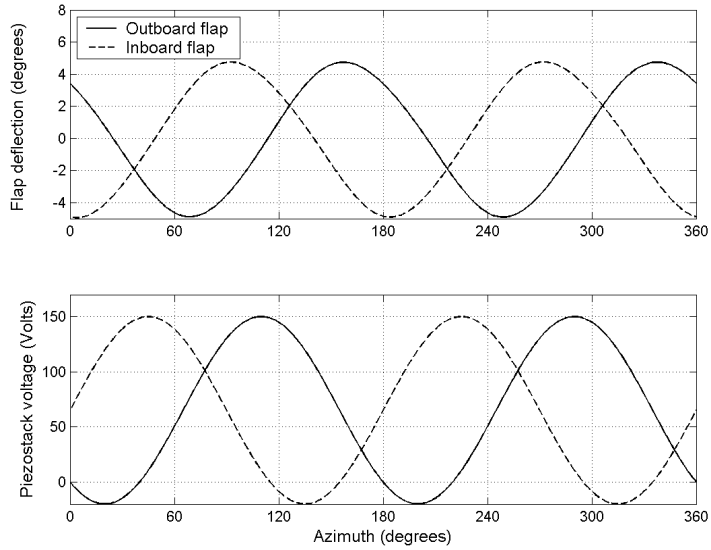

Figure 9: Optimal 2/rev control input and resulting flap motion

Figure 10 shows the optimal 3/rev control input and the resulting flap motion of both flaps. The optimal inboard and outboard flap motions are nearly out-of-phase. The actuator output in this case lags the control input by about 41 degrees for both flaps. Again, this phase difference is due to the actuator hysteresis and is non-negligible. The aeroelastic analysis predicts a reduction of about 78 percent in hub vibration. The 4/rev longitudinal, lateral and vertical hub shear forces are reduced by about 43, 38 and 67 percent from their respective baseline values. The 4/rev rolling, pitching and yawing hub moments are reduced by about 28, 34 and 50 percent from their respective baseline values.

The optimal 4/rev control input and the resulting flap motion for the inboard and outboard flaps are shown in Figure 11. In this case, the inboard flap leads the outboard flap motion by about 37 degrees. The actuator output in this case lags the control input by about 36 degrees for both flaps. The hub vibration levels are reduced by about 66 percent from the baseline values. Figure 12 shows the reduction in the individual 4/rev hub loads for the three cases considered above. . It is worth noting that in all three control input cases, both flaps have the same amplitude but different phasing with respect to the rotor azimuth. This amplitude corresponds to the maximum actuator stroke at respective actuation frequency.

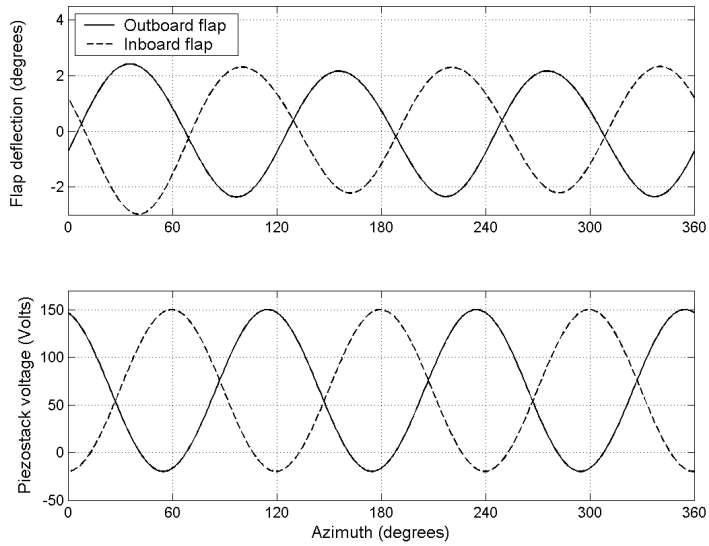

Figure 10: Optimal 3/rev control input and resulting flap motion

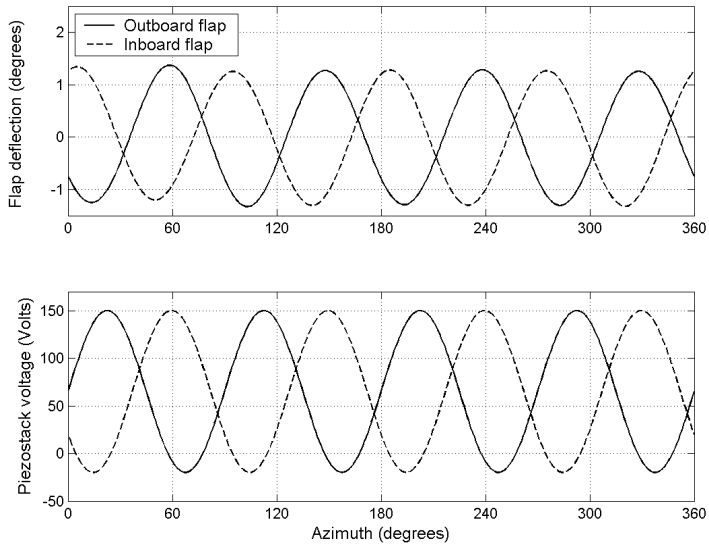

Figure 11: Optimal 4/rev control input and resulting flap motion

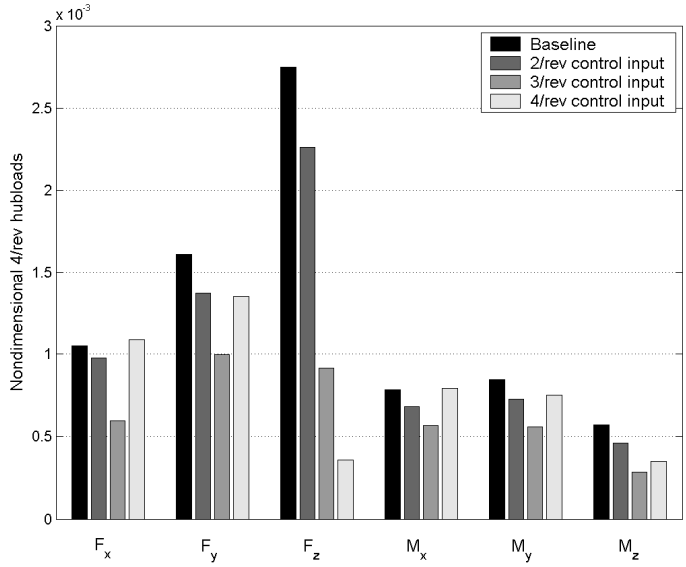

Figure 12: Comparison of 4/rev hub forces and moments

7 CONCLUSIONS

In this study, the effect of piezoceramic actuator hysteresis on helicopter vibration control using trailing-edge flaps is studied. An aeroelastic model of the helicopter with multiple trailing-edge flaps is used to predict the hub vibration levels at different flight conditions. A commercially available piezoceramic stack actuator suited for full-scale trailing-edge flap actuation is experimentally tested on a bench-top apparatus. Experimental results show that the actuator is fairly nonlinear even under quasi-static conditions. Moreover, the nonlinear behavior of the actuator varies with the actuation frequency, i.e., the amplitude and phasing of the actuator output is a function of both voltage amplitude and frequency.

The hysteresis in the stack actuator is modeled using a dynamic hysteresis model based on an extension of the classical Preisach model. Experimental data obtained using the bench-top test is used to determine the unknown parameters in the actuator dynamic hysteresis model. This model is then compared with experimental results from higher actuation frequency and it is found that the dynamic hysteresis effects are captured very well.

The "feedback form of the global controller"' is used to determine the optimal control input at individual 2, 3, and 4Ω harmonics. Active vibration control is simulated for steady-state high forward speed flight condition. It is seen that the phase difference between the actuator output (flap motion) and the input (applied voltage) is typically about 32-40 degrees. This phase difference is non-negligible and is due to the presence of actuator hysteresis. The magnitude of this phase difference depends directly on the amplitude and frequency of the input voltage. Ignoring the dynamic hysteresis in the stack actuator or using a linear model for the actuator will almost certainly lead to erroneous prediction in the optimal control input. This in turn will lead to non-optimal flap motion which will directly affect the performance of the trailing-edge flap system.

8 REFERENCES

[1] P. P. Friedmann, "Vibration reduction in rotorcraft using actively controlled flaps –

From theoretical concept to flight ready software", Proceedings of the CEAS/AIAA/NVvL International Forum on Structural Dynamics and Aeroelasticity, Amsterdam, The Netherlands, June 4-6, 2003.
[2] N. Koratkar and I. Chopra, "Closed-loop wind tunnel testing of a smart rotor model with trailing-edge flaps", Journal of the American Helicopter Society, Vol. 47, No. 4, 2002, pp. 263-272.
[3] J. S. Kim, E. C. Smith, and K. W. Wang, "Helicopter vibration suppression via multiple trailing edge flaps controlled by resonance actuation system", in Proceedings of the 60th Annual Forum of the American Helicopter Society, Baltimore, Maryland, USA, June 2004.
[4] T. Lee and I. Chopra, "Design of piezostack-driven trailing edge flap actuator for helicopter rotors", Smart Materials and Structures, Vol. 10, No. 1, 2001, pp. 15-24.
[5] S. R. Hall and E. F. Prechtl, "Preliminary testing of a Mach-scaled active rotor blade with a trailing-edge servo flap", Proceedings of SPIE Conference on Smart Structures and Materials, Newport Beach, CA, USA, 1999, pp. 14-21.
[6] A. J. Kurdila, J. Li, T. Strganac and G. Webb, "Nonlinear control methodologies for hysteresis in PZT actuated on-blade elevons", Journal of Aerospace Engineering, Vol. 16, No. 4, 2003, pp. 167-176.
[7] S. R. Viswamurthy and R. Ganguli, "Effect of piezoelectric hysteresis nonlinearity on helicopter vibration control using trailing-edge flaps," Proceedings of the 46th AIAA/ASME/ASCE/AHS/ASC Structures, Structural Dynamics and Materials Conference, Austin, Texas, USA, 18-21 April 2005.
[8] F. Preisach, "On magnetic aftereffect," Zeitschrift für Physiks, Vol. 94, 1935, pp. 277-302.
[9] J. G. Leishman and T. S. Beddoes, "A semi-empirical model for dynamic stall", Journal of the American Helicopter Society, Vol. 34, No. 3, 1989, pp. 3-17.
[10] N. Hariharan and J. G. Leishman, "Unsteady aerodynamics of a flapped airfoil in subsonic flow by indicial concepts", Journal of Aircraft, Vol. 33, No. 5, 1996, pp. 855-868.
[11] A. Bagai and J. G. Leishman, "Rotor free-wake modeling using a pseudo-implicit technique including comparisons with experiment", Journal of the American Helicopter Society, Vol. 40, No. 3, 1995, pp. 29-41.
[12] S .R. Viswamurthy and R. Ganguli, "An optimization approach to vibration reduction in helicopter rotors with multiple active trailing edge flaps", Aerospace Science and Technology, Vol. 8, No. 3, 2004, pp. 185-194.
[13] M. A. Krasnoselskii and A. V. Pokrovskii, Systems with Hysteresis, Springer-Verlag, New York, 1989, pp.1-57.
[14] I. D. Mayergoyz, "Hysteresis models from the mathematical and control theory points of view", Journal of Applied Physics, Vol. 57, No. 8, 1985, pp. 3803-3805.
[15] I. D. Mayergoyz, "On numerical implementation of hysteresis models", IEEE Transactions on Magnetics, Vol. 21, No. 5, 1985, pp. 1853-1855.
[16] P. N. Sreeram and N. G. Naganathan, "Hysteresis prediction for a piezoceramic material system", Proceedings of 1993 ASME Winter Annual Meeting, New Orleans, LA, 1993, pp. 35-42.
[17] D. Hughes and J. T. Wen, "Preisach modeling of piezoceramic and shape memory alloy hysteresis", Smart Materials and Structures, Vol. 6, No. 3, 1997, pp. 287-300.
[18] P. Ge and M. Jouaneh, "Modeling hysteresis in piezoceramic actuators", Precision Engineering, Vol. 17, No. 3, 1995, pp. 211-221.
[19] I. D. Mayergoyz, "Dynamic Preisach models of hysteresis", IEEE Transactions on Magnetics, Vol. 24, No. 6, 1988, pp. 2925-2927.
[20] W. Johnson, "Self-tuning regulators for multicyclic control of helicopter vibration",

NASA Technical Paper-1996, March 1982.
[21] P. P. Friedmann and T. A. Millott, “Vibration reduction in rotorcraft using active control: A comparison of various approaches”, Journal of Guidance, Control and Dynamics, Vol. 18, No. 4, 1995, pp. 664-673.
[22] T. A. Millott and P. P. Friedmann, “Vibration reduction in helicopters rotors using an actively controlled partial span trailing edge flap located on the blade”, NASA CR-4611, June 1994.